Acta Crystallographica Section B
Structural Science
ISSN 0108-7681

$KSm(MoO_4)_2$, an incommensurately modulated and partially disordered scheelite-like structure

Alla Arakcheeva,[a]* Philip Pattison,[a,b] Gervais Chapuis,[a] Marta Rossell,[c] Andrey Filaretov,[a] Vladimir Morozov[d] and Gustaaf Van Tendeloo[c]

[a]École Polytechnique Fédérale de Lausanne, Laboratoire de Cristallographie, BSP, CH-1015 Lausanne, Switzerland, [b]Swiss–Norwegian Beamline, ESRF, BP-220, F-38043 Grenoble CEDEX, France, [c]EMAT, University of Antwerp, Groenenborgerlaan 171, B-2020 Antwerp, Belgium, and [d]Department of Chemistry, Moscow State University, 119899 Moscow, Russia

Correspondence e-mail: alla.arakcheeva@epfl.ch

Received 6 December 2007
Accepted 17 January 2008

The incommensurately modulated scheelite-like $KSm(MoO_4)_2$ structure has been refined in the monoclinic superspace group $I2/b(\alpha\beta0)00$ by the Rietveld method on the basis of synchrotron radiation powder diffraction data. The systematic broadening of satellite reflections has been accounted for by applying anisotropic microstrain line-broadening. The microstructure has been studied by transmission electron microscopy (TEM). The partial disorder of the K and Sm cations in the *A* position is best approximated by a combination of harmonic and complex crenel functions with (0.952Sm + 0.048K) and (0.952K + 0.048Sm) atomic domains. This combination yields a compositional wave distribution from $\{KMoO_4\}$ to $\{SmMoO_4\}$ observed in the *ab* structure projection along **q**. The specific features of $KSm(MoO_4)_2$ and degree of the *A*-cation ordering are discussed in comparison with the previously reported structure of $KNd(MoO_4)_2$.

1. Introduction

The design and functioning of solid-state lasers as new advanced devices for optoelectronic applications is the focus of increasing attention (Volkov *et al.*, 2005; Cerny *et al.*, 2002; Pask & Piper, 2000). The $A(XO_4)$ compounds with scheelite and scheelite-like structures (Fig. 1) are considered with regard to their self-doubling solid-state laser host properties. For this reason the crystal structures and optical properties of $MR(XO_4)_2$ [*M* = alkali metal; *X* = Mo, W; *R* is a trivalent rare-earth element (REE)] have been extensively studied (Volkov *et al.*, 2005; Neeraj *et al.*, 2004; Shimamura *et al.*, 2002; Cheng *et al.*, 2001; Shi *et al.*, 1998). The optical properties are closely related to the symmetry of its crystal structure. As reported earlier (Morozov *et al.*, 2006), the $KNd(MoO_4)_2$ scheelite-like structure can only be correctly solved and described as incommensurately modulated using (3 + 1)D superspace-group symmetry. A range of compounds [tetragonal $AgNd(WO_4)_2$ reported by Colòn *et al.* (2005); $LiYb(MoO_4)_2$ reported by Volkov *et al.* (2005); $NaLa(MoO_4)_2$ and $NaCe(MoO_4)_2$ reported by Teller (1992)] and some other compounds exhibit X-ray powder diffraction (XRPD) patterns containing weak low-angle reflections, which have been neglected in the refinement and ignored in the corresponding discussions. These reflections cannot be indexed with the proposed unit-cell parameters and point to modulated structures. The modulated character of the structures can also be recognized for some scheelite-like compounds registered in the ICDD database with incomplete lists of *hkl* indexes [for example, $KLa(MoO_4)_2$, ICDD-PDF No. 40-0466, and $KEu(MoO_4)_2$, ICDD-PDF No. 31-1006]. Therefore, the modulated character of the structure is not a rare phenomenon for scheelite-like compounds and its proper refinement

with superspace symmetry seems to be an important component of the characterization of the prospective laser material. However, the modulated nature and the higher-dimensional symmetry of these compounds has never been applied to the optical property analysis because an incommensurately modulated structure has been reported for $KNd(MoO_4)_2$ only.

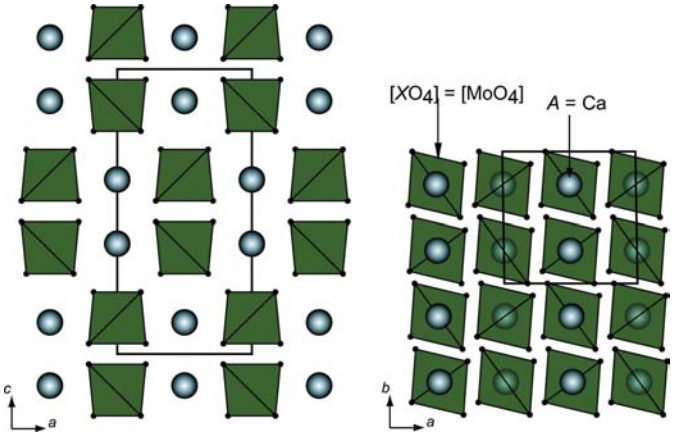

Figure 1
The scheelite-like monoclinic structure. The high-pressure modification of $CaMoO_4$ (space group $I112/b$; a = 5.108, b = 5.034, c = 10.768 Å, γ = 90.96°; Crichton & Grzechnik, 2004) is shown in the *ab* and *ac* projections. The scheelite-like unit cell is indicated.

The present work deals with the refinement of the new incommensurately modulated structure $KSm(MoO_4)_2$. This structure exhibits a partially disordered distribution of K and Sm on the *A* position in contrast to a completely ordered $KNd(MoO_4)_2$ scheelite-like structure, aperiodic in three dimensions, as previously reported (Morozov *et al.*, 2006). The structure has been refined by the Rietveld method on the basis of synchrotron powder diffraction data. The systematic broadening of satellite reflections has been accounted for by applying the anisotropic microstrain line-broadening (AMLB) model (Elcombe & Howard, 1988; Rodriguez-Carvajal *et al.*, 1991; Popa, 1998; Stephens, 1999; Leineweber, 2007). Originally introduced for the description of a three-dimensional powder diffraction profile, it has been recently generalized by Leineweber & Petříček (2007) for (3 + 1)D incommensurately modulated structures. The *JANA*2006 program package adapted for this aim (Petříček *et al.*, 2006) has been used for the present refinement. In order to trace the advantages of the AMLB model, all steps of the structure refinement have been performed with and without this improvement using the *JANA*2006 and *JANA*2000 program packages, respectively.

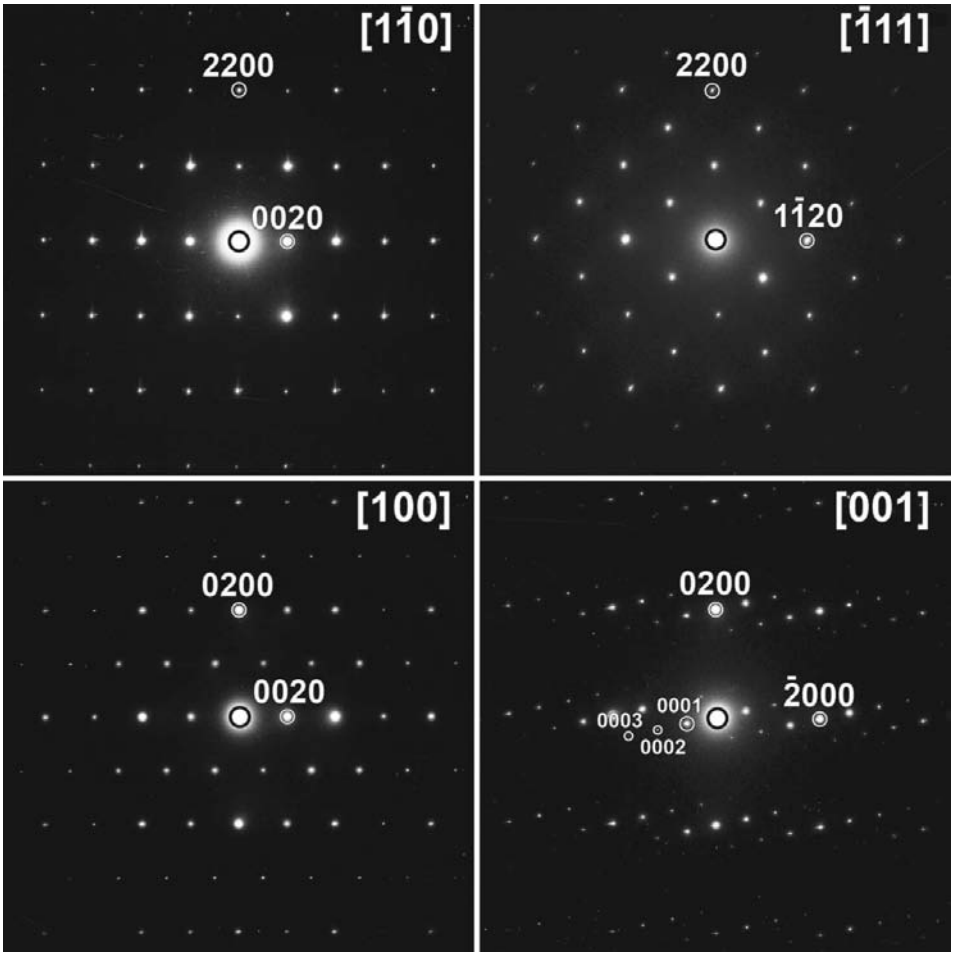

Figure 2
Electron diffraction patterns along the main zone axes for the incommensurately modulated $KSm(MoO_4)_2$ phase.

2. Experimental

2.1. Preparation

The $KSm(MoO_4)_2$ double molybdenum oxide was prepared from a (1:1:4) stoichiometric mixture of K_2CO_3 (99.99%), Sm_2O_3 (99.99%) and MoO_3 (99.99%) by a routine ceramic technique at 953–973 K for 80 h in air followed by quenching from 973 K to room temperature. The title compound is the only phase present, as confirmed by synchrotron powder diffraction analysis.

2.2. Electron diffraction study

Electron diffraction (ED) and high-resolution electron microscopy (HREM) investigations were made on crushed samples deposited on carbon grids. Energy-dispersive X-ray (EDX) analysis and ED patterns were obtained using a CM20 Philips microscope with a LINK-2000 attachment. The element composition of $KSm(MoO_4)_2$ was confirmed by EDX analysis performed inside the transmission electron microscope

and linked with the ED analysis for each crystallite. EDX was performed at three points each for ten different crystallites. The K:Sm:Mo cation ratio was 0.97 (14):1.06 (15):2.00 [24 (2) at. % K, 26 (2) at. % Sm, 50 (4) at. % Mo] and it is close to the bulk $KSm(MoO_4)_2$ composition.

The [1$\bar{1}$0], [1$\bar{1}\bar{1}$], [100] and [001] ED patterns of $KSm(MoO_4)_2$ (Fig. 2) are very similar to those reported

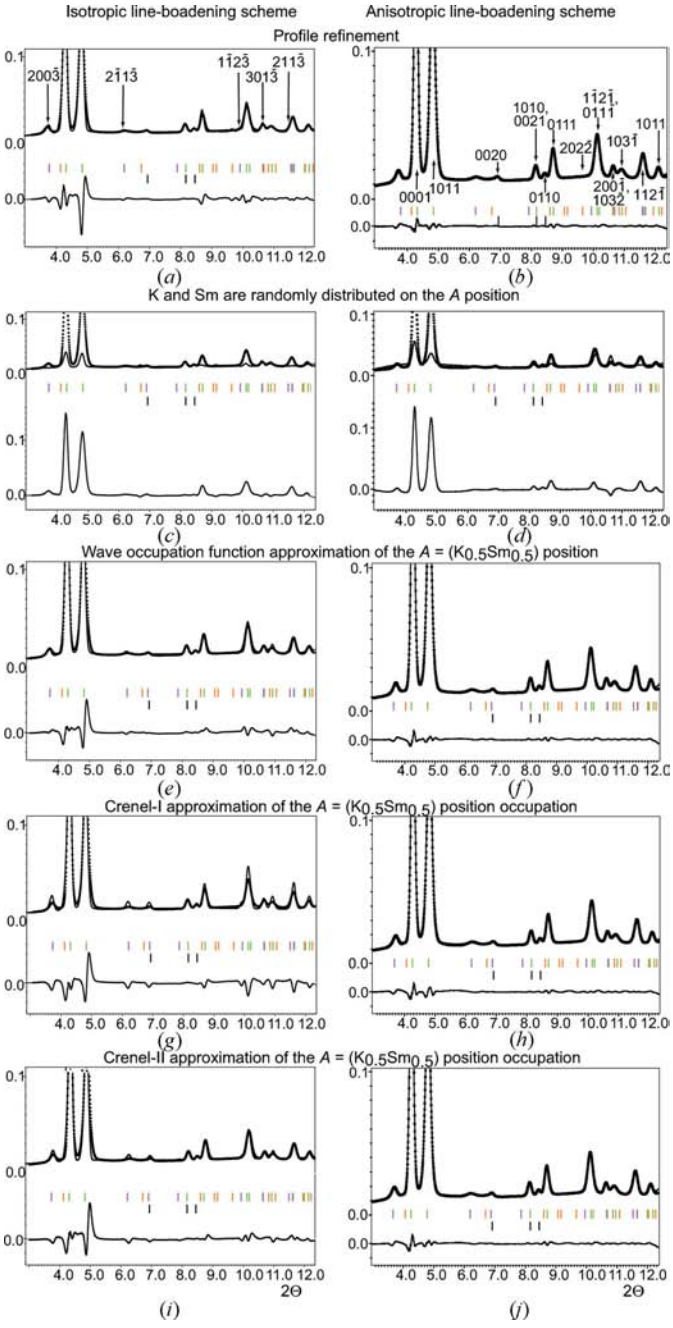

Figure 3
Illustration of the different model refinements performed from synchrotron experimental data for $KSm(MoO_4)_2$. The lower-angle part of the diffraction pattern is shown. The stars refer to experimental patterns, while the solid lines correspond to calculated and difference patterns. Le Bail decomposition has not been applied. Tick marks denote the peak positions of the possible Bragg reflections: black marks for the main reflections, green, orange and pink marks for the first-, second- and third-order satellites, respectively.

Table 1
Experimental details.

Crystal data	
Chemical formula	$KSm(MoO_4)_2$
M_r	509.3
Cell setting, space group	Monoclinic, $I2/b(\alpha\beta0)00$
Temperature (K)	273
a, b, c (Å)	5.5279 (2), 5.2994 (2), 11.7841 (1)
γ (°)	91.1388 (5)
V (Å^3)	345.15
Z	2
D_x (Mg m^{-3})	4.899
Modulation wavevector	$\mathbf{q} = 0.56771\ (5)\mathbf{a}^* - 0.12682\ (8)\mathbf{b}^*$
Radiation type	Synchrotron
Specimen form, colour	Capillary, yellow
Specimen size (mm)	0.5 mm
Specimen preparation cooling	By quenching from 973 to 293 K in air
Specimen preparation pressure (kPa)	101.325
Specimen preparation temperature (K)	293
Data collection	
Diffractometer	MAR345
Data collection method	Specimen mounting: glass capillary; mode: transmission; scan method: IPDS
2θ (°)	$2\theta_{min} = 1.998$, $2\theta_{max} = 40.798$, increment = 0.005
Refinement	
Refinement on	F
R factors and goodness-of-fit	$R_p = 0.025$, $R_{wp} = 0.035$, $R_{exp} = 0.000$, $S = 1.10$
Wavelength of incident radiation (Å)	0.7114
Excluded region(s)	None
Profile function	Pseudo-Voigt
No. of parameters	42
Weighting scheme	Based on measured s.u.'s
$(\Delta/\sigma)_{max}$	0.002

Computer programs used: *JANA*2006 (Petříček *et al.*, 2006).

previously for $KNd(MoO_4)_2$ (Fig. 3 in Morozov *et al.*, 2006). All reflections in the [1$\bar{1}$0], [1$\bar{1}\bar{1}$] and [100] ED patterns are main reflections referring to the tetragonal scheelite unit cell with parameters $a_t \simeq 5.40$, $c_t \simeq 11.80$ Å. The larger part of weaker reflections observed in the [001] ED pattern are satellite reflections which can be indexed with four *hklm* integers, as given by the diffraction vector $\mathbf{H} = h\mathbf{a}^* + k\mathbf{b}^* + l\mathbf{c}^* + m\mathbf{q}$, with the modulation vector $\mathbf{q} \simeq 0.57\mathbf{a}_t^* - 0.13\mathbf{b}_t^*$ and $m \neq 0$. The reflections with $m = 0$ and $m \neq 0$ correspond to the main and satellite reflections, respectively. Since the **q** vector components are significantly different from any rational value, the structure can be considered as incommensurately modulated.

The position of the satellites in the [001] ED pattern is similar to the corresponding pattern of $KNd(MoO_4)_2$, also requiring a monoclinic symmetry. In analogy to $KNd(MoO_4)_2$, the pseudo-tetragonal I-centered scheelite-like unit cell and the monoclinic superspace group $I2/b(\alpha\beta0)00$ have been proposed for $KSm(MoO_4)_2$.

All ED patterns (Fig. 2) can be completely indexed in the superspace group $I2/b(\alpha\beta0)00$ with the unique c axis. The [1$\bar{1}$0], [1$\bar{1}\bar{1}$] and [100] diffraction patterns exhibit only main

Table 2
Characteristics of the profile refinement for $KSm(MoO_4)_2$.

	Main reflections		Main reflections and satellites up to the first order		Main reflections and satellites up to the second order		Main reflections and satellites up to the third order	
	1	2	3	4	5	6	7	8
R_p	0.1470	0.1221	0.0410	0.0142	0.0333	0.0129	0.0288	0.0092
R_{wp}	0.2546	0.2243	0.0726	0.0250	0.0591	0.0237	0.0539	0.0144
GOF	7.46	6.73	2.13	0.75	1.73	0.71	1.58	0.43

Columns 1, 3, 5 and 7 refer to the refinements performed without accounting for an anisotropic microstrain line-broadening; columns 2, 4, 6 and 8 refer to the refinements performed with the anisotropic microstrain line-broadening model.

*hkl*0 reflections. The [$1\bar{1}0$] and [$1\bar{1}\bar{1}$] patterns exhibit *hk*00: h, $k \neq 2n$ reflections forbidden by the *I*2/*b* symmetry. Their intensities are, however, systematically lower than the *hk*00 intensities with h, $k = 2n$. On tilting the sample around the [*hk*00] direction, the reflections *hk*00: h, $k \neq 2n$ further weaken and finally vanish in the [001] pattern. Consequently, these spots are attributed to double diffraction and do not violate the *I*2/*b* symmetry. Besides the I-centring reflections, all satellite reflections (*hk*0*m*) with $k = 2n + 1$ are extinct.

2.3. Crystal structure study

Rietveld analysis of the incommensurately modulated scheelite-like structure of $KSm(MoO_4)_2$ was performed in the superspace group $I2/b(\alpha\beta0)00$ using the *JANA*2000 and *JANA*2006 program packages (Petříček *et al.*, 2000, 2006). The main details of the experiment and characteristics of the final structure refinement are listed in Table 1. All illustrations were produced with the *JANA*2000 and *JANA*2006 program packages in combination with the program *DIAMOND* (Brandenburg, 1999).

2.3.1. Synchrotron diffraction experiment and profile refinement. The powder diffraction experimental data set was obtained at room temperature with a MarResearch MAR345 image-plate area detector using synchrotron radiation on beamline BM01A (SNBL) at the ESRF, Grenoble [λ = 0.7114 Å, Si(111) monochromator and focusing mirrors]. Diffraction patterns were collected at sample–detector distances of 200 mm. The sample was contained in a 0.5 mm-diameter capillary, which was rotated through 30° during an exposure of 30 s per image.

The powder diffraction data cover the range $1.998 \leq 2\theta \leq 40.80°$ with steps of 0.005°. The refinement of the unit-cell constants along with the profile parameters allowed the indexing of 174 main reflections and satellites up to the third order. The lower-angle range ($1.998 \leq 2\theta \leq 12.3°$) of the diffraction pattern, where some single satellites are resolved, is shown in Fig. 3 in order to trace different stages of the structure investigation starting from the profile refinement. In this range, only three weak main reflections are present, while the first-order satellites are the strongest ones; the third-order satellites, especially 200$\bar{3}$, are also clearly visible.

The quality of the profile refinement depends strongly on the order of the satellites included in the refinement and on the method of the line approximation (Table 2). The refinements without satellites and including satellites up to first, second and third order have been performed. Two methods of the line-shape description have been considered, representing eight cases in total. The first method uses the conventional isotropic line broadening (ILB). The second method involves the anisotropic microstrain line-broadening (AMLB) proposed by Leineweber & Petříček (2007). The profile refinement characteristics obtained with the ILB method are systematically worse (odd columns in Table 2) than those obtained with the AMLB method (even columns in Table 2). If only the main reflections are included, the fit is poor (first and second columns in Table 2). The first-order satellites radically improve the profile characteristics (third and fourth columns in Table 2). Including second-order satellites further improves the profile (fifth and sixth columns in Table 2). The best profile approximation is obtained by taking into account satellites up to third order (seventh and eighth columns in Table 2). The advantage of the AMLB profile approximation (eighth column in Table 2) over the ILB one (seventh column in Table 2) is also illustrated in Fig. 3 (top). In order to trace the influence of the anisotropic microstrain line-broadening on the incommensurately modulated structure refinement, both versions, with ILB and AMLB, have been reported at each stage during the structure investigation (Table 3, Fig. 3). The ILB version originates from the *JANA*2000 program package, while the *JANA*2006 program package has been exploited for the AMLB calculations. All refinements were performed including satellites up to third order.

The comparison of the unit-cell parameters and the **q** vector [a = 5.527942 (17), b = 5.299372 (15), c = 11.78431 (4) Å, γ = 91.1389 (2)°, **q** = 0.56776 (1)**a*** − 0.126803 (6)**b***] obtained from the refinement of the profile reveals a good agreement with the electron microscopy results.

2.3.2. Structure refinement. The set of Mo and O atomic parameters (including the first-order Fourier amplitudes of the displacive modulation function) obtained for $KNd(MoO_4)_2$ (Morozov *et al.*, 2006) and two atoms, K and Sm, statistically occupying the A position (x_1 = 0.5, x_2 = 0.25, x_3 = 0.88) were used as initial parameters for the refinement of the modulated $KSm(MoO_4)_2$ structure. The displacive modulation functions [the first-order Fourier amplitudes for Mo, O and for A = ($K_{0.5}Sm_{0.5}$) position] along with coordinates and isotropic atomic displacement parameters (ADPs) were refined. For both ILB and AMLB methods, this model gives acceptable values of $R \simeq 0.05$ for main reflections and higher values of

Table 3
Characteristics of the different model refinements for $KSm(MoO_4)_2$.

	Crenel approximation of the $A = (K_{0.5}Sm_{0.5})$ position occupation				Wave approximation of the $A = (K_{0.5}Sm_{0.5})$ position occupation		Combination of the crenel-II and a wavefunction for the $A = (K_{0.5}Sm_{0.5})$ position occupation	
	Crenel-I: o[K] = 1, o[Sm] = 0 ($0 < t < 0.5$); o[Sm] = 1, o[K] = 0 ($0.5 < t < 1$)		Crenel-II: o[K] = 1 − δ, o[Sm] = δ ($0 < t < 0.5$); o[Sm] = 1 − δ, o[K] = δ ($0.5 < t < 1$)					
	1	2	3	4	5	6	7	8
R_p	0.0592	0.0282	0.0471	0.0249	0.0483	**0.0248**	0.0475	**0.0248**
R_{wp}	0.0864	0.0402	0.0747	**0.0350**	0.0714	0.0352	0.0743	0.0350
GOF	2.54	1.21	2.19	**1.05**	2.09	1.06	2.18	1.05
R; wR (all, obs)	0.0374; 0.0280	0.0158; 0.0180	0.0279; 0.0198	0.0137; 0.0159	0.0280; 0.0194	0.0139; 0.0160	0.0274; 0.0196	**0.0135**; **0.0155**
R; wR (main, obs)	0.0194; 0.0183	0.0131; 0.0197	0.0151; 0.0134	0.0117; 0.0179	0.0156; 0.0129	0.0115; 0.0179	0.0155; 0.0134	**0.0115**; **0.0174**
R; wR (1, obs)	0.0482; 0.0312	0.0180; 0.0197	0.0341; 0.0209	0.0151; 0.0182	0.0355; 0.0208	0.0160; 0.0186	0.0331; 0.0208	**0.0152**; **0.0179**
R; wR (2, obs)	0.0562; 0.0302	0.0196; 0.0179	0.0505; 0.0230	0.0174; 0.0146	0.0471; 0.0236	**0.0169**; **0.0143**	0.0471; 0.0231	0.0173; 0.0142
R; wR (3, obs)	0.0600; 0.0309	0.0148; 0.0138	0.0442; 0.0212	0.0130; 0.0120	0.0406; 0.0195	0.0125; 0.0124	0.0408; 0.0205	**0.0127**; **0.0117**
No. of atomic ref. par.	39	39	40	40	42	42	41	41
ρ_{max}, ρ_{min} (e Å^{-3})	1.84; −1.39	0.30; −0.27	0.99; −1.12	0.20; −0.21	0.81; −0.81	0.20; −0.24	0.97; −1.0	**0.19**; **−0.20**

Columns 1, 3, 5 and 7 refer to the refinements performed without accounting for an anisotropic microstrain line-broadening; columns 2, 4, 6 and 8 refer to the refinements performed with an anisotropic microstrain line-broadening model, $\delta = 0.090$ (2), 0.048 (1), 0.095 (1) and 0.054 (1) for columns 3, 4, 7 and 8, respectively. Bold font indicates the most relevant value of each parameter.

$R \simeq 0.06$–0.15 for satellites, but unacceptably high values of profile parameters, $R_p \simeq 0.12$, $R_{wp} \simeq 0.20$ and GOF $\simeq 6$. Further improvement of the profile characteristics results in a large increase of the O and (K,Sm) displacive modulations, which leads to both increasing of all structural R factors and unreasonable variations of the (K,Sm)—O distances from 1.6 to 4.2 Å. Thus, independently of the method of the line-shape approximation, the refinement of the model with K and Sm randomly distributed on the A position shows only a small contribution to the intensities of satellites, assuming reasonable displacive atomic modulations. This is illustrated with the lower-angle range of the diffraction pattern presented in the corresponding part of Fig. 3.

The electron and residual electron density calculated in the vicinity of the $A = (K_{0.5}Sm_{0.5})$ position (Fig. 4) showed that the half-average occupancy approximation for the K and Sm distribution along the internal axis, x_4, is not correct. The maxima (~ 5 e Å^{-3}) of the residual electron density (Fig. 5, bottom) point to the concentration of the 'heavier' Sm atom around $x_4 = 0.5$, while the minima (~ -5 e Å^{-3}) indicate the concentration of the 'lighter' K atom around $x_4 = 0$. The continuous variation from ~ 50 to ~ 80 e Å^{-3} of the electron density distribution along the x_4 axis (Fig. 5, top) indicates the wavy behaviour of the A position occupation by K and Sm.

According to this estimation, two complementary waves of the A position occupation with the occupancy coefficient $o = 0.5$ were used for K and Sm for further refinement. In this context, the term 'wave' is defined as a limited series of lowest-order harmonic terms. Initially, the fractional coordinates and ADPs of the two atoms were constrained to be identical. Later, this condition was removed and the second harmonic term of the Sm displacive modulation was introduced. The first harmonic term of the occupation waves was successfully refined with the Fourier amplitude close to 0.5 referring to two complementary sinusoidal waves. At this stage the structural R factors (especially for the main reflections and the first-order satellites) and the profile parameters decreased globally. Refinement of the second harmonic of the occupation waves did not affect the results noticeably, while the third harmonic essentially improved the whole set of the refinement characteristics (Table 3, columns 5 and 6). The higher fit of both profile and structure refinement relates to the AMLB method (Table 3, column 6 and Fig. 3*f*) in comparison with the ILB one (Table 3, column 5 and Fig. 3*e*). The values of the refined S'_{HKLM} coefficients of the polynomial describing AMLB [see equation (21) and Table 2 reported by Leineweber & Petříček, 2007] are listed in Table 4, column 1.

The resulting function of the A position occupation is in good agreement with the K and Sm displacive modulations, and the corresponding residual electron density varies smoothly from −0.1 to 0.1 e Å^{-3} (Fig. 5*a*).

In the $0.1 < t < 0.4$ and $0.6 < t < 0.9$ ranges (Fig. 5*a*), the occupations of Sm (95%) and K (95%) are probably constant. The slightly wavy shape of the occupation functions is probably an artefact owing to the limited number of harmonic terms. In this case, the wave approximation of the K and Sm distribution in the A position (Fig. 5*a*) is reminiscent of a crenel function. This fact encouraged us to perform a refinement with K and Sm distributions approximated by crenel functions (Fig. 5*b*): o[K] = 1 and o[Sm] = 0 in $0 < t < 0.5$;

Table 4
The S'_{HKLM} coefficients of the polynomial describing AMLB refined for different models of the A position occupation in $KSm(MoO_4)_2$.

HKLM in S'_{HKLM}	Wave approximation of the $A = (K_{0.5}Sm_{0.5})$ position occupation	Crenel-I: o[K] = 1, o[Sm] = 0 ($0 < t < 0.5$); o[Sm] = 1, o[K] = 0 ($0.5 < t < 1$)	Crenel-II: o[K] = 0.953, o[Sm] = 0.047 ($0 < t < 0.5$); o[Sm] = 0.953, o[K] = 0.047 ($0.5 < t < 1$)
*HKL*0			
4000	−0.064 (6)	−0.064 (4)	−0.062 (4)
0400	−0.107 (7)	−0.118 (5)	−0.112 (5)
0040	−0.00027 (8)	−0.00036 (7)	−0.00030 (7)
2200	0.043 (3)	0.036 (2)	0.043 (2)
1300	−0.026	−0.033 (2)	−0.028 (3)
3100	−0.006 (2)	0.006 (2)	−0.005 (2)
1120	0.0033 (4)	0.0026 (2)	0.0032 (2)
2020	−0.0060 (4)	−0.0051 (4)	−0.0062 (4)
0220	0.0034 (3)	0.0045 (3)	0.0036 (3)
*HKL*1			
3001	0.14 (2)	0.09 (3)	0.06 (1)
2101	−0.14 (1)	−0.33 (2)	−0.15 (1)
1201	0.16 (2)	0.25 (2)	0.15 (2)
1021	−0.175 (8)	−0.16 (1)	−0.155 (8)
0301	−0.20 (4)	−0.13 (5)	−0.27 (4)
0121	0.07 (1)	0.14 (2)	0.098 (1)
*HKL*2			
0022	1.49 (2)	1.70 (2)	1.50 (2)
0202	−0.03 (5)	−0.04 (6)	−0.02 (4)
2002	0.32 (2)	0.40 (3)	0.38 (2)
1102	−0.58 (3)	−0.64 (4)	−0.60 (3)

o[Sm] = 1 and o[K] = 0 in $0.5 < t < 1$. The diffraction pattern calculated for the crenel-I model with the ILB method (Fig. 3*g*) reveals an overestimation of the intensities for satellites. However, a reasonable profile fit is obtained with the AMLB method (Fig. 3*h*). The profile parameters and characteristics of the structure refinement, including the magnitude of the residual electron density (Table 3, columns 1 and 2), can also be considered as reasonable for this crenel-I model. However, they are significantly worse in comparison with the wave occupation function model (Table 3, columns 5 and 6 for the ILB and AMLB methods, respectively). The higher magnitude of the residual electron density calculated in the vicinity of the A position (Fig. 5) also points to a preference of the wave-occupation function model (Fig. 5*a*) over the crenel-I model (Fig. 5*b*). The values of the refined coefficients S'_{HKLM} of the polynomial describing AMLB (Table 4, column 2) are very close to those refined for the wave occupation function model (Table 4, column 1).

The crenel-I model has been improved (Table 3, column 4) by refining the amplitudes of the crenel functions and applying the AMLB method {o[K1] = 0.952 (1) and o[Sm2] = 0.048 (1) in the $0 < t < 0.5$ range; o[Sm1] = 0.952 (1) and o[K2] = 0.048 (1) in the $0.5 < t < 1$ range}. The following obvious restrictions have been applied in this model: the coordinates (x, y, z), ADPs and displacive modulations of K1 and K2 have been restricted to be equal; the same has been done for Sm1 and Sm2; o[K1] = o[Sm1] = 1 − o[Sm2], o[Sm2] = o[K2]. Hence, only one additional refined parameter, namely o[Sm1], has been included in comparison with the crenel-I model. The lower-angle diffraction pattern corresponding to the crenel-II (AMLB) model (Fig. 3*j*) and the values of the refined S'_{HKLM} coefficients of the polynomial describing AMLB (Table 4, column 3) are very similar to the wave-occupation function model (Table 4, column 1). Residual electron density maps calculated in the vicinity of the A position are also similar to the wave-approximation model (*cf.* Figs. 5*a* and 5*c*).

The next model of refinement tested involves both refined amplitudes of the crenel functions and one harmonic term of the occupation modulation for the A position. In this combined model, the value of the harmonic term amplitude has been restricted to be equivalent for Sm1, Sm2, K1 and K2, but with the opposite sign for K and Sm atoms. The resulting refined occupation functions are shown in Fig. 5(*d*), for the AMLB method. For this model, the quality of the profile approximation and the accuracy of structure refinement are the best (Table 3, column 8) and the number of refined parameters is intermediate between the crenel-II and the wave-approximation models. The residual electron density maps

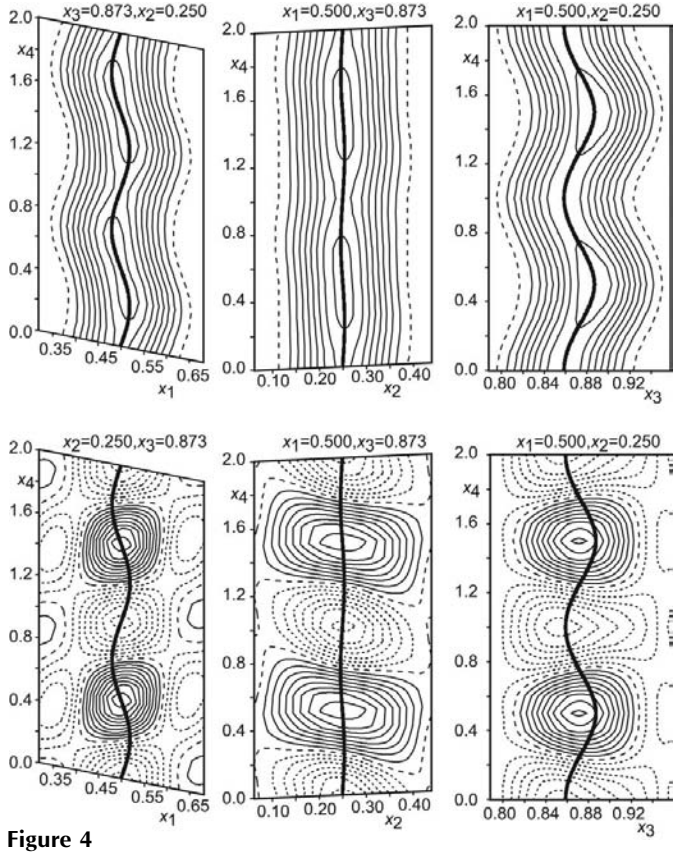

Figure 4
The vicinity of the $A = (K_{0.5}Sm_{0.5})$ position in the structural model with randomly distributed K and Sm atoms. The x_1–x_4, x_2–x_4 and x_3–x_4 sections are presented for electron density (top) and residual electron density (bottom) maps. Full, dashed and dotted lines show positive, zero and negative values of the electron density. The step between lines is 10 and 0.5 e Å^{-3} for electron and residual electron density, respectively. The central lines correspond to calculated displacive modulation functions.

calculated close to the *A* position (Fig. 5*d*) exhibit the smallest magnitude. The refined S'_{HKLM} coefficients of the polynomial describing AMLB are identical within less than one standard deviation to those of the crenel-II model (Table 4, column 3).

2.3.3. Selection of the structural model. In the previous paragraphs we have described the refinements of four structure models. Only the refinements with the AMLB method will be considered in this section, owing to the poor profile approximation with the ILB method (Table 3, Fig. 3). The four models described only differ by the function of the *A* position occupation. The displacive modulations of the *A* position are approximately identical for those models in the ranges $0 < t < 0.5$ and $0.5 < t < 1$ occupied by Sm (< 95%) and K (< 95%), respectively (Fig. 5). Comparison of the refinement char-

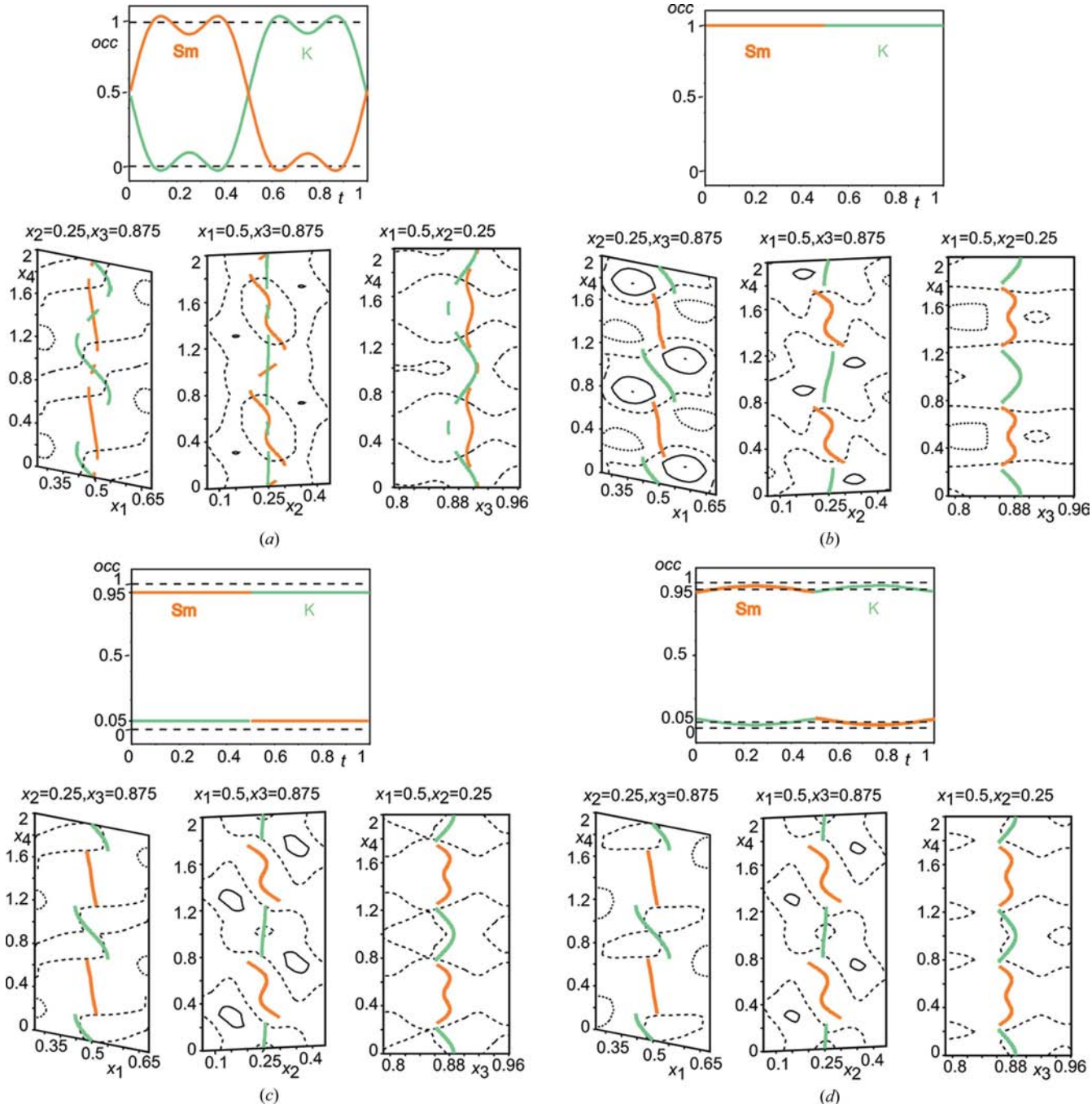

Figure 5
The occupation modulation functions and corresponding displacive modulations of Sm and K in the *A* position of $KSm(MoO_4)_2$ for (*a*) the wave occupation function, (*b*) the crenel-I, (*c*) the crenel-II and (*d*) the combined models. For the four occupation functions, the x_1–x_4, x_2–x_4 and x_3–x_4 sections are presented for residual electron density maps. Full, dashed and dotted black lines show positive, zero and negative values of the electron density, respectively. The step between the lines is 0.1 e Å^{-3}. The central lines correspond to calculated displacive modulation functions; the colours of the lines indicate ranges of K and Sm with respect to the occupation function. The dashed ranges of the colour lines in (*a*) indicate the ranges with low concentration (< 10%) of K and Sm. On the other maps, the colours indicate the range with more than 94% occupation of the corresponding atom.

Table 5
Final coordinates, isotropic displacement parameters and Fourier amplitudes of the displacive modulation function for $KSm(MoO_4)_2$.

The waves are sorted by the term *s* for sines, *c* for cosines and order *n*. The values reported by Morozov *et al.* (2006) for $KNd(MoO_4)_2$ are shown in brackets for comparison.

	Occupation	Wave	*x*	*y*	*z*	U_{eq} (Å^2)
K1	0.473K1 +		0.5	0.25	0.8774 (5)	0.029 (1)
K2	0.027K2				[0.8892 (11)]	
[K]						
		s,1	−0.037 (8)	0.004 (1)	0	
		c,1	0	0	0.007 (1)	
Sm1	0.473Sm1 +		0.5	0.25	0.8757 (1)	0.0010 (3)
Sm2	0.027Sm2				[0.8797 (18)]	
[Nd]						
		s,1	0.00809 (19)	0.0116 (3)	0	
		c,1	0	0	−0.0019 (8)	
		s,2	0.015 (4)	0.0152 (4)	0	
		c,2	0	0	0.0038 (4)	
Mo	1		0.5	0.25	0.37796 (8)	0.0101 (3)
					[0.3774 (2)]	
		s,1	0.0335 (2)	−0.0059 (2)	0	
			[0.0289 (7)]	[−0.0048 (7)]		
		c,1	0	0	0.0140 (1)	
					[0.0109 (4)]	
O1	1		0.3539 (3)	0.0114 (4)	0.2917 (2)	0.0071 (17)
			[0.3599 (10)]	[0.0203 (12)]	[0.2928 (5)]	
		s,1	0.0264 (8)	0.0090 (9)	−0.0119 (4)	
			[0.027 (3)]	[0.008 (3)]	[−0.0005 (12)]	
		c,1	0.0013 (9)	0.0261 (9)	0.0073 (3)	
			[−0.001 (3)]	[0.020 (3)]	[0.0070 (11)]	
O2	1		0.7654 (5)	0.3982 (4)	0.0420 (2)	0.0198 (9)
			[0.7744 (13)]	[0.3936 (10)]	[0.0429 (5)]	
		s,1	0.0159 (8)	−0.0272 (10)	0.0004 (4)	
			[0.023 (2)]	[−0.021 (3)]	[0.0029 (12)]	
		c,1	0.0352 (7)	0.0157 (11)	−0.0066 (4)	
			[0.030 (3)]	[−0.004 (3)]	[−0.0030 (12)]	

K1 and Sm2 are defined for $-0.25 < x_4 < 0.25$ with the Fourier amplitude of the occupation modulation wave equal to −0.0116 (3) and 0.0116 (3), respectively; Sm1 and K2 are defined for $0.25 < x_4 < 0.75$ with the Fourier amplitude of the occupation modulation wave equal to 0.0116 (3) and −0.0116 (3), respectively.

acteristics (Table 3) indicates that the crenel-I model referring to a complete ordering of K and Sm on the *A* position can be discarded for further consideration as the profile characteristics and accuracy of the refinement are significantly better when a partially disordered distribution of K and Sm are taken into account. It is difficult to give a preference between the remaining models describing partial disordering on the *A* position. The characteristics of refinement (Table 3) remain approximately identical in different refinements for the wave, crenel-II and the combined models, respectively. In these models, the displacive modulations are approximated with two harmonic terms for the Sm and one for the K, Mo and O atoms. The total number of refined structural parameters differs by one or two units only (40, 41 and 42). A comparison of Figs. 5(*d*), 5(*c*) and 5(*a*) points to the *A* position occupation changing continuously and sharply from mainly Sm to mainly K atomic domains. More harmonic terms are needed in the combined model to approximate this sharp change. Since all structural parameters, except the occupation modulation function, are identical for the three considered models within one standard deviation, selecting one of them does not significantly affect the overall results of the analysis. The combined occupation function model has been selected as the final structural data for $KSm(MoO_4)_2$ because of the intermediate number of refined parameters, 41, and the better accuracy of the structure refinement (Table 3, column 8).

For this model, the crystallographic parameters, atomic coordinates and modulation parameters, and selected interatomic distances are listed in Tables 1, 5 and 6; displacive modulations of Mo and O atoms along the x_4 axis are illustrated in Fig. 6; modulations of the K—O, Sm—O and Mo—O interatomic distances are shown in Fig. 7 as a function of the *t* axis. The calculated and difference powder diffraction patterns are presented in Fig. 8 for the whole 2θ range of the experimental data. A portion of the incommensurately modulated $KSm(MoO_4)_2$ structure is shown in Fig. 9 in the *ab* projection.[1]

2.4. High-resolution electron microscopy observation

The quality of the structure solution is confirmed by HREM observations, performed using a Jeol 4000 EX microscope operating at 400 kV. The Scherzer resolution of the microscope is 1.7 Å.

HREM observations were performed at room temperature along the [001] direction. An image and the corresponding Fourier transform (FT) pattern are shown in Fig. 10 (top). The FT pattern exhibits a spot distribution similar to that of the ED pattern in Fig. 2, indicating that the modulation features have been imaged.

3. Discussion

3.1. Advantages of the anisotropic microstrain line-broadening application

The microstrain-like anisotropic diffraction line-broadening concept developed for (3 + 1)D incommensurately modulated phases (Leineweber & Petříček *et al.*, 2006) has been applied here in parallel to the standard ILB description of the diffraction lines. The advantage of the AMLB method for the profile approximation is evident from Table 2 and Fig. 3. The higher accuracy of the profile approximation using the AMLB method (R_P = 0.0092, R_{wp} = 0.0144) allows the refinement of structural models with a much higher accuracy (Table 3, even columns) than analogous refinement using the ILB method scheme (Table 3, odd columns).

It should be noted that this advantage did not help us propose a more precise conclusion about the preferred structural model. Using either the AMBL or the ILB method,

[1] Supplementary data for this paper are available from the IUCr electronic archives (Reference: SN5063). Services for accessing these data are described at the back of the journal.

Table 6
Selected A—O (A = K, Sm) and Mo—O distances (Å) and angles (°) in the [MoO_4] tetrahedra in $KSm(MoO_4)_2$.

	Average	Minimal	Maximal
K1—O1	2.707 (16)	2.285 (12)	2.913 (15)
K1—O1	2.713 (16)	2.295 (12)	2.913 (15)
K1—O1	2.70 (3)	2.36 (2)	2.86 (4)
K1—O1	2.71 (3)	2.37 (2)	2.86 (4)
K1—O2	2.60 (3)	2.50 (3)	2.80 (2)
K1—O2	2.60 (3)	2.50 (3)	2.80 (2)
K1—O2	2.693 (14)	2.495 (15)	2.826 (12)
K1—O2	2.690 (14)	2.494 (15)	2.826 (12)
Sm1—O1	2.458 (11)	2.362 (11)	2.686 (8)
Sm1—O1	2.467 (11)	2.362 (11)	2.699 (8)
Sm1—O1	2.435 (17)	2.33 (2)	2.569 (12)
Sm1—O1	2.428 (17)	2.321 (12)	2.566 (12)
Sm1—O2	2.535 (17)	2.426 (18)	2.840 (11)
Sm1—O2	2.545 (17)	2.426 (18)	2.861 (11)
Sm1—O2	2.485 (11)	2.365 (11)	2.763 (9)
Sm1—O2	2.492 (11)	2.365 (11)	2.786 (9)
Mo—O1	1.807 (5)	1.765 (5)	1.849 (5)
Mo—O1	1.807 (5)	1.765 (5)	1.849 (5)
Mo—O2	1.803 (5)	1.775 (5)	1.832 (5)
Mo—O2	1.804 (5)	1.775 (5)	1.831 (5)
O1—Mo—O1	111.1 (2)	106.6 (2)	116.0 (2)
O1—Mo—O2	107.9 (2)	102.5 (2)	113.1 (3)
O1—Mo—O2	106.4 (2)	105.0 (2)	107.3 (2)
O1—Mo—O2	114.00 (14)	110.16 (14)	117.96 (14)
O1—Mo—O2	115.85 (15)	111.77 (15)	119.77 (15)
O2—Mo—O2	116.9 (2)	109.0 (2)	125.1 (3)

both the profile and the structural refinement characteristics of the completely ordered structural model (Table 3, columns 1 and 2) are significantly worse than those of the three other models describing a partially disordered structure with three different occupation functions of the A position. Using either the AMLB or the ILB scheme, it was not possible to select the best partially disordered model. Perhaps this selection is beyond the limits of the powder diffraction technique.

The application of the AMLB method allows also some estimation of the microstrain distribution in the $KSm(MoO_4)_2$ incommensurately modulated phase. Nine S'_{HKL0} and ten S'_{HKLM} parameters with $H+K+L+M=4$ have been refined (Table 4) according to the monoclinic symmetry with a two-component **q** vector (Table 2 in Leineweber & Petříček, 2007). According to Leineweber & Petříček (2007), if the anisotropic microstrain distribution is the real origin of the anisotropic broadening of the diffraction lines, then the values of S'_{HKL0} and S'_{HKL2} refer to a variation of the average unit-cell parameters and the **q** vector, respectively; correlation between a, b, c and the **q** vector affects S'_{HKL1}. The values of S'_{HKL0} (Table 4) are close to zero; hence they indicate that the average unit-cell parameters are rather constant. The values of S'_{HKL2} (Table 4) are the highest among other S'_{HKLM} coefficients; therefore, variations of the **q** vector are mainly responsible for the satellite line-broadening observed in the experiment (Fig. 8). The condition for the isotropic microstrain distribution is $S'_{2002}/(\alpha_{200})^2 = S'_{0202}/(\alpha_{020})^2 = S'_{0022}/(\alpha_{002})^2$ and $S'_{1102} = 0$, where $\alpha_{200} = \mathbf{a}^*\cdot\mathbf{a}^*$, $\alpha_{020} = \mathbf{b}^*\cdot\mathbf{b}^*$, $\alpha_{002} = \mathbf{c}^*\cdot\mathbf{c}^*$ (Leineweber & Petříček, 2007). In this case, the unit-cell parameters $a \simeq b \simeq 0.5c$ and the monoclinic angle γ is close to 90° (Table 1); consequently, $16(\alpha_{200})^2 \simeq 16(\alpha_{020})^2 \simeq (\alpha_{002})^2$. Hence, the main condition for isotropy is $S'_{0022} = 16S'_{2002} = 16S'_{0202}$. The refined values $S'_{0022} \simeq 4S'_{2002}$ and $S'_{0202} \simeq 0$ (Table 4) indicate anisotropic variation of the α and γ components of the **q** vector, α being more variable than γ, while the β component is constant. Such a variation is associated with an ellipsoidal symmetry of the microstrain distribution in the ac plane, while minimal microstrains are associated with the b axis. This observation can be interpreted as an ellipsoidal precession of the **q** vector around the b axis.

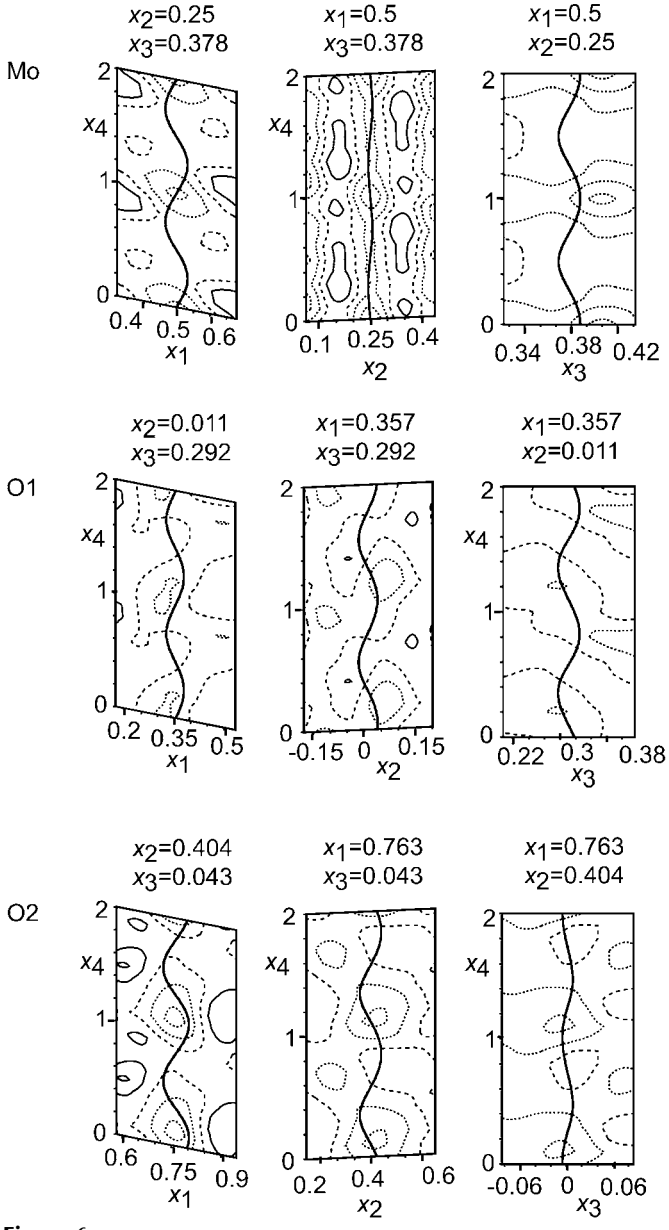

Figure 6
Displacive modulations of Mo and O atoms in $KSm(MoO_4)_2$. Results of the combined occupation function model refinement have been used for calculation of the x_1–x_4, x_2–x_4 and x_3–x_4 sections of the residual electron density. The step between lines is 0.1 e Å^{-3}. The central bold lines correspond to the calculated atomic positions.

3.2. Specific structural features of the incommensurately modulated $KSm(MoO_4)_2$ in comparison with $KNd(MoO_4)_2$

The refined structure of $KSm(MoO_4)_2$ is very similar to our previously reported structure $KNd(MoO_4)_2$ (Morozov *et al.*, 2006). Both structures belong to the same superspace group $I2/b(\alpha\beta0)00$ with closely related unit-cell parameters and **q** vectors [*cf.* Table 1 and characteristics of $KNd(MoO_4)_2$: a = 5.5202 (2), b = 5.33376 (5), c = 11.8977 (3) Å, γ = 90.9591 (7)°, **q** = 0.57789 (4)**a*** − 0.14748 (6)**b***]. The coordinates of the corresponding atoms differ by less than 3 standard uncertainties for Sm and Mo, and less than 10 standard uncertainties for K and O atoms (Table 5). The origin of the structure modulation is also identical for the two structures. This is due to an ordered distribution of different cations on the *A* position of the scheelite-like structure (Fig. 9 and Fig. 6 in Morozov *et al.*, 2006). This distribution is related to a compositional wave propagating in the *ab* plane in the direction of the **q** vector (Figs. 9 and 10 compared with Fig. 10 reported by Morozov *et al.*, 2006). The compositional wave changing from $\{K(MoO_4)\}$ to $\{Ln(MoO_4)\}$ (Ln = Nd, Sm) is periodic with the length equal to $1/|\mathbf{q}| = 1/|\alpha\mathbf{a}^* + \beta\mathbf{b}^*|$), but incommensurate relating to the *a* and *b* unit-cell parameters, owing to the irrationality of α and β. The result of the superposition of two periodic functions (the continuous compositional wave and the discrete framework of the *A* positions; Fig. 9) gives an aperiodic discrete function (distribution of K and Ln on *A* positions) as a consequence of the irrational ratio of their periodicities. The main difference between the $KSm(MoO_4)_2$ and $KNd(MoO_4)_2$ structures refers to the difference of the compositional wavefunction, which is

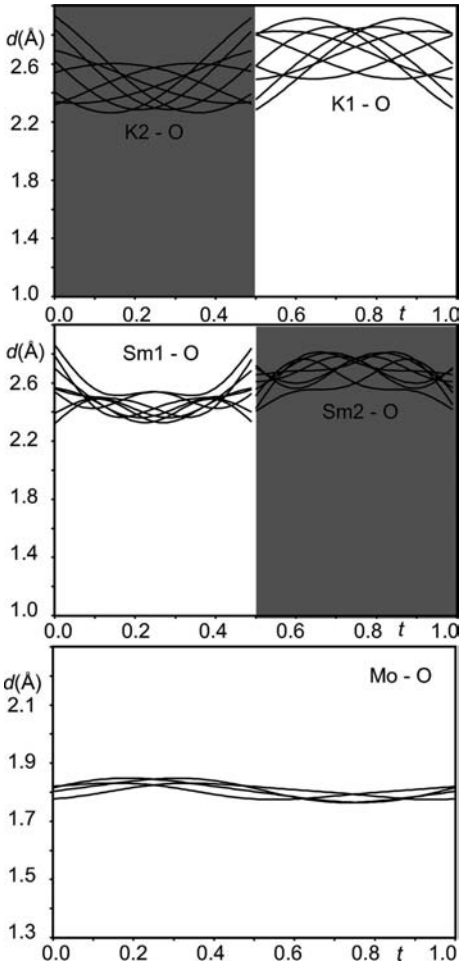

Figure 7
Distances K—O, Sm—O and Mo—O as a function of *t*. The dark areas indicate the distance sets with a low, < 5%, probability of presence.

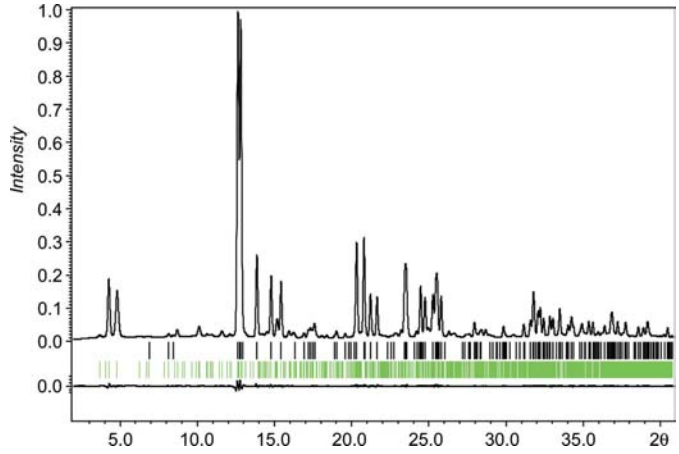

Figure 8
Profile and difference synchrotron diffraction patterns calculated on the basis of synchrotron data for the refinement of $KSm(MoO_4)_2$ with the combined occupation function model. Tick marks denote the peak positions of possible Bragg reflections: black marks for the main reflections, green marks for satellites. All characteristics of the refinement are listed in Tables 1 and 3, column 8.

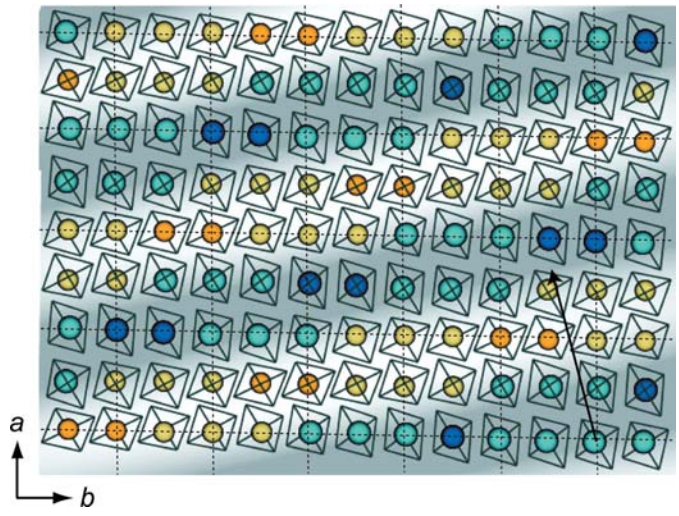

Figure 9
A portion of the $KSm(MoO_4)_2$ aperiodic structure in the *ab* projection. The green and yellow spheres indicate $A = (K_{1-x}Sm_x)$ positions for $x < 0.5$ and $x > 0.5$, respectively. The $[MoO_4]$ tetrahedra are represented by their edges. The grey and white wave indicates the continuously changing chemical composition from mainly $\{K[MoO_4]\}$ (centre of the grey part) to mainly $\{Sm[MoO_4]\}$ (centre of the white part). The direction and length of this wave (arrow) is parallel to the **q** vector with length $1/|\mathbf{q}|$. Darker spheres indicate mainly K ($x < 0.01$) and mainly Sm ($x > 0.99$) *A* positions. The *a* and *b* unit-cell translations are indicated for the *A* site by dashed lines.

defined by the occupation modulation function of the A position. Two typical crenel functions (100% K atomic domain and 100% Nd atomic domain) describe K and Nd in $KNd(MoO_4)_2$. Similar domains, (95% K + 5% Sm) and (95% Sm + 5% K), are slightly doped by the 'foreign' cation in $KSm(MoO_4)_2$ (see §2.3.3 and Fig. 5). The crenel functions completely describe the ordered $KNd(MoO_4)_2$ structure, where A = K or Nd, whereas the best models of the $KSm(MoO_4)_2$ structure describe a partially disordered distribution of K and Sm. In the latter case, the composition of A is always mixed, $A = (K_{1-x}Sm_x)$, and the x value is probably changing continuously from ~ 0.01 ($A \simeq K_{0.99}Sm_{0.01}$) to ~ 0.95 ($A \simeq Sm_{0.99}K_{0.01}$) and back (see §2.3.3 and Fig. 9). The partially disordered distribution of K and Sm might be linked to the variation of the **q** vector considered above.

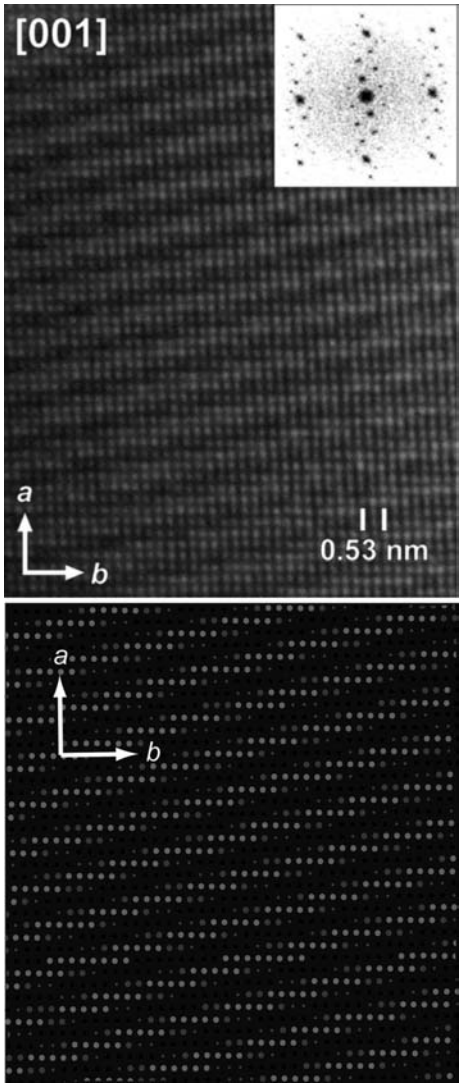

Figure 10
[001] HREM image and corresponding Fourier transformation pattern (upper part) compared with a schematic representation of the structure portion (lower part) of the incommensurately modulated $KSm(MoO_4)_2$. In the structure presentation, the $A = (K_{1-x}Sm_x)$ positions are shown as circles decorated by a grey colour gradation from lightest grey ($x < 0.05$) to darkest grey ($x > 0.95$).

In accordance with the compositional wave, the A—O distances continuously vary from the minimal value, $\langle Sm1—O\rangle \simeq \langle K2—O\rangle \simeq 2.40$ Å, to the maximal one, $\langle K1—O\rangle \simeq \langle Sm2—O\rangle \simeq 2.75$ Å (Fig. 7). Similar to $KNd(MoO_4)_2$, the A—O distance variation is due to the displacive modulation of the A cations and the $[MoO_4]$ tetrahedron (Fig. 11). The accompanying distortion of this tetrahedron is larger in $KSm(MoO_4)_2$ (Table 6, Fig. 7) than in $KNd(MoO_4)_2$ (Table 4 and Fig. 7 in Morozov *et al.*, 2006): in $KSm(MoO_4)_2$, the Mo—O distances are slightly increased, varying from 1.77 to 1.85 Å, and the O—Mo—O angles dispersed from 102.5 to 125.1°, while in $KNd(MoO_4)_2$, the Mo—O distances are more typical, 1.69–1.83 Å, and the O—Mo—O angles are less dispersed, 105.6–120.7°.

3.3. On the stabilization of the scheelite-like modulated structures with different degrees of *A*-cation ordering

As mentioned above, the ordering of different cations in the A position of the scheelite-like modulated structures is associated with displacements of the A cations and the $[MoO_4]$ tetrahedra resulting in proper A—O distances for specific A cations. In the absence of any ordering, the higher symmetrical phases with scheelite structure type (space group $I4_1/a$, $a \simeq$

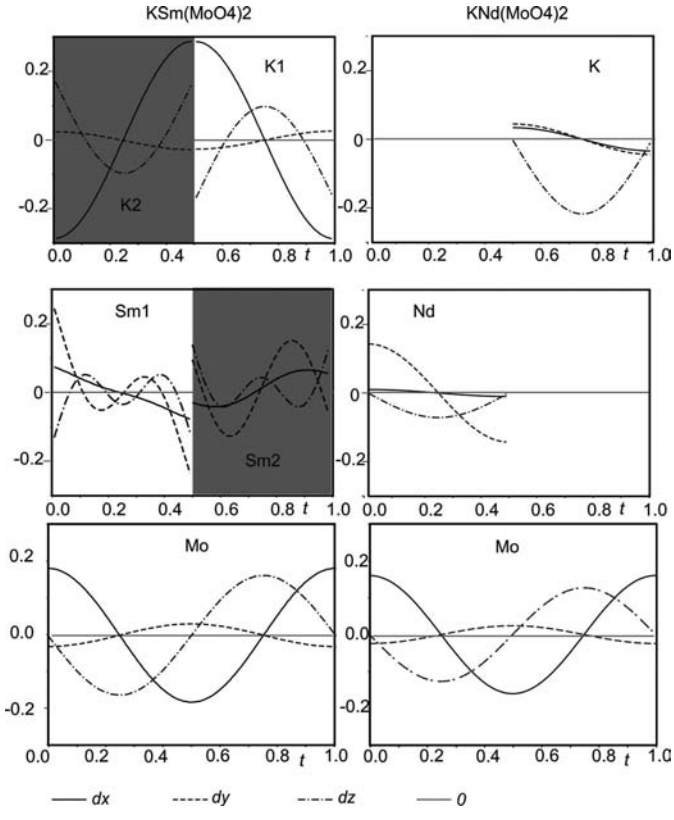

Figure 11
Fractional displacements from the average position of Mo and Ln (Sm, Nd) atoms in the incommensurately modulated structures $KSm(MoO_4)_2$ and $KNd(MoO_4)_2$. The dark areas indicate the displacements with a low probability of presence: < 7% for K—O and < 12% for Sm—O, respectively, in the K and Sm plots.

5.5 Å, $c \simeq 2a$) are usually adopted for $MR(XO_4)_2$, where M = alkali metal, R = REE; X = Mo, W, Cr and some others [for instance, $LiY(MoO_4)_2$ and $LiNd(MoO_4)_2$ reported by Kolitsch (2001)]. In these phases, the M and R atoms are randomly distributed on the A position and $A-O$ distances correspond to the (M,R) statistical composition. Hence, no displacements of X from its special position (x, y and z are fixed) have been observed. In ordered structures, it is evident that the displacements of A cations and the $[MoO_4]$ tetrahedra have to be proportional to the difference in the characteristic $M-O$ and $R-O$ distances for different A cations. Therefore, one would expect a complete ordering of M and R cations if this difference is smaller and, hence, the building unit displacements require less energy for the ordered phase stabilization. This hypothesis is confirmed by comparing the incommensurately modulated structures $KSm(MoO_4)_2$ and $KNd(MoO_4)_2$. The maximal difference between $\langle K-O\rangle \simeq 2.75$ Å and $\langle Nd-O\rangle \simeq 2.55$ Å in $KNd(MoO_4)_2$ [Fig. 7 in (Morozov *et al.*, 2006)] is significantly less than the maximal difference between $\langle K-O\rangle \simeq 2.75$ Å and $\langle Sm-O\rangle \simeq 2.40$ Å in $KSm(MoO_4)_2$ (Fig. 7). In accordance with this observation, a complete separation of K and Nd is reached in $KNd(MoO_4)_2$ and only a partial ordering of K and Sm appears in $KSm(MoO_4)_2$, along with approximately identical displacements of $[MoO_4]$ from their average position in both structures (Fig. 11). As follows from the $KNd(MoO_4)_2$ structure, these displacements can support only ~ 0.2 Å maximal differences in the $A-O$ distances, and the observed ~ 0.35 Å has been reached in $KSm(MoO_4)_2$ owing to much larger displacements of the A cations (Fig. 11) and the increase in the Mo—O distances in the larger distorted $[MoO_4]$ tetrahedron, as mentioned above.

4. Conclusions

The second incommensurately modulated scheelite-like structure, $KSm(MoO_4)_2$, has been refined in the superspace group $I2/b(\alpha\beta0)00$. The superspace group, unit-cell parameters, **q** vector, fractional atomic coordinates and origin of the structure modulations are very similar to those of the previously reported structure $KNd(MoO_4)_2$. The main specific feature of $KSm(MoO_4)_2$ is the partially disordered distribution of K and Sm atoms on the A site in contrast to $KNd(MoO_4)_2$, where K and Nd are completely ordered. This behaviour is linked to a compensating mechanism associated with different K—O and Ln—O (Ln = Sm and Nd) distances.

This investigation shows that even a partially disordered, incommensurately modulated structure can be successfully refined from powder diffraction data using a combination of synchrotron radiation together with the tools available in *JANA*2006. The obvious difference in peak widths observed among the satellite reflections can be attributed to the anisotropic microstrain line-broadening scheme for the profile refinement.

We would like to thank Lukáš Palatinus for his helpful discussion on the interpretation of the refined values of the S'_{HKLM} coefficients of the polynomial describing AMLB. The contribution of the Swiss National Science foundation, grant No. 20-105325/1, is gratefully acknowledged. We are grateful to the Swiss–Norwegian beamline consortium for the provision of synchrotron radiation facilities.

References

Brandenburg, K. (1999). *DIAMOND*, Version 2.1c. Crystal Impact GbR, Bonn, Germany.
Cerny, P., Jelinkova, H., Basiev, T. T. & Zverev, P. G. (2002). *IEEE J. Quantum Electron.* **38**, 1471–1478.
Cheng, Z., Lu, Q., Zhang, S., Liu, J., Yi, X., Song, F., Kong, Y., Han, J. & Chen, H. (2001). *J. Cryst. Growth*, **222**, 797–800.
Colòn, C., Alonso-Medina, A., Fernàndez, F., Sàez-Puche, R., Volkov, V., Casales, C. & Zaldo, C. (2005). *Chem. Mater.* **17**, 6635–6643.
Crichton, W. A. & Grzechnik, A. (2004). *Z. Kristallogr. New Cryst. Struct.* **219**, 337–338.
Elcombe, M. M. & Howard, C. J. (1988). *Mater. Sci. Forum*, **27–28**, 71–76.
Kolitsch, U. (2001). *Z. Kristallogr.* **216**, 449–454.
Leineweber, A. (2007). *J. Appl. Cryst.* **40**, 362–370.
Leineweber, A. & Petříček, V. (2007). *J. Appl. Cryst.* **40**, 1027–1034.
Morozov, V. A., Arakcheeva, A. V., Chapuis, G., Gublin, N., Rossell, M. D. & Van Tendeloo, G. (2006). *Chem. Mater.* **18**, 4075–4082.
Neeraj, S., Kijima, N. & Cheetham, A. K. (2004). *Chem. Phys. Lett.* **387**, 2–6.
Pask, H. M. & Piper, J. A. (2000). *IEEE J. Quantum Electron.* **36**, 949–955.
Petříček, V., Dušek, M. & Palatinus, L. (2000). *JANA*2000. Institute of Physics, Praha, Czech Republic.
Petříček, V., Dušek, M. & Palatinus, L. (2006). *JANA*2006. Institute of Physics, Praha, Czech Republic.
Popa, N. C. (1998). *J. Appl. Cryst.* **31**, 176–180.
Rodriguez-Carvajal, J., Fernandez-Diaz, M. T. & Martinez, J. L. (1991). *J. Phys. Condens. Matter*, **3**, 3215–3234.
Shi, F., Meng, J., Ren, Y. & Su, Q. (1998). *J. Phys. Chem. Solids*, **59**, 105–110.
Shimamura, K., Sato, H., Bensalah, A., Machida, H., Sarukura, N. & Fukuda, T. (2002). *Opt. Mater.* **19**, 109–116.
Stephens, P. W. (1999). *J. Appl. Cryst.* **32**, 281–289.
Teller, R. G. (1992). *Acta Cryst.* C**48**, 2101–2104.
Volkov, V., Cascales, C., Kling, A. & Zaldo, C. (2005). *Chem. Mater.* **17**, 291–300.